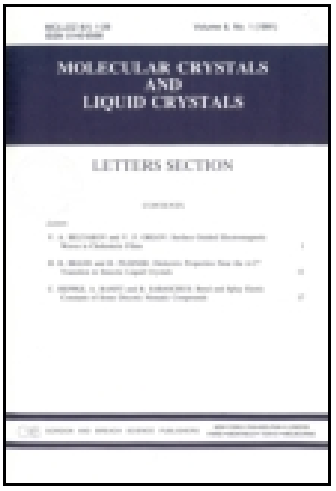

Molecular Crystals and Liquid Crystals
Publication details, including instructions for authors and subscription information:
http://www.tandfonline.com/loi/gmcl20

Enhancing Photoelectrical Performance of Dye-Sensitized Solar Cell Using Phosphor Photoelectrode

Seong Gwan Shin[a], Kyung Hwan Kim[a], Chung Wung Bark[a] & Hyung Wook Choi[a]

[a] Department of Electrical Engineering, Gachon University, Sujeong-Gu, Seongnam-Si, Gyeonggi-Do, Korea

Published online: 06 Dec 2014.

To cite this article: Seong Gwan Shin, Kyung Hwan Kim, Chung Wung Bark & Hyung Wook Choi (2014) Enhancing Photoelectrical Performance of Dye-Sensitized Solar Cell Using Phosphor Photoelectrode, Molecular Crystals and Liquid Crystals, 602:1, 96-103, DOI: 10.1080/15421406.2014.944682

To link to this article: http://dx.doi.org/10.1080/15421406.2014.944682

Mol. Cryst. Liq. Cryst., Vol. 602: pp. 96–103, 2014

ISSN: 1542-1406 print/1563-5287 online
DOI: 10.1080/15421406.2014.944682

Taylor & Francis
Taylor & Francis Group

Enhancing Photoelectrical Performance of Dye-Sensitized Solar Cell Using Phosphor Photoelectrode

SEONG GWAN SHIN, KYUNG HWAN KIM, CHUNG WUNG BARK, AND HYUNG WOOK CHOI*

Department of Electrical Engineering, Gachon University, Sujeong-Gu, Seongnam-Si, Gyeonggi-Do, Korea

Dye-sensitized solar cells (DSSCs) are composed of an electrode made of a dye-adsorbed nanoporous TiO_2 layer on a fluorine-doped tin oxide (FTO) glass substrate, redox electrolytes, and a counter electrode. In this study, phosphor is introduced into the TiO_2-layer electrode in a DSSC. By a conversion luminescence, YAG:Ce^{3+} phosphor improves light harvesting and increases the photocurrent production. Using a TiO_2 electrode containing 5.00 wt% mixed YAG:Ce^{3+}, the light-to-electric energy conversion efficiency of the DSSC reaches 6.24%, which is higher by a factor of 1.52 than that of a DSSC without YAG:Ce^{3+}.

Keywords DSSC; phosphor; luminescence; TiO_2; nanoparticle; YAG:Ce^{3+}

Introduction

Dye-sensitized solar cells (DSSCs) have been intensively studied since their discovery in 1991 [1–7]. DSSCs have been attracting considerable attention around the world because of their reasonable conversion efficiency, low production cost, and simple fabrication process compared to silicon solar cells [8–16]. A DSSC is composed of an electrode made of a dye-adsorbed nanoporous TiO_2 layer on a fluorine-doped tin oxide (FTO) glass substrate, redox electrolytes, and a counter electrode. One of the ways to increase the efficiency of DSSC is to enhance the harvest of light [17–19]. Many synthetic dyes have been synthesized and employed to improve the harvest of light and increase photocurrent production by DSSCs; however, even the best dyes (N-719) only absorbs in the wavelength range 400–800 nm, [20–21] and most of the ultraviolet wavelength are not used. If ultraviolet and broad region irradiation can be converted to absorption band of dye by a conversion luminescence and can be reabsorbed by the dye in the DSSC, more solar irradiation can be used, and the photocurrent of the DSSC will be effectively enhanced.

In this work, the $Y_3Al_5O_{12}$:Ce^{3+}(YAG:Ce^{3+}) phosphor is introduced into the DSSC to improve light harvesting, photocurrent production, and solar conversion efficiency by a

*Address correspondence to Prof. Hyung Wook Choi, Department of Electrical Engineering, Gachon University, Sujeong-Gu, Seongnam-Si, Gyeonggi-Do, Korea (ROK). E-mail: chw@Gachon.ac.kr

Color versions of one or more of the figures in the article can be found online at www.tandfonline.com/gmcl.

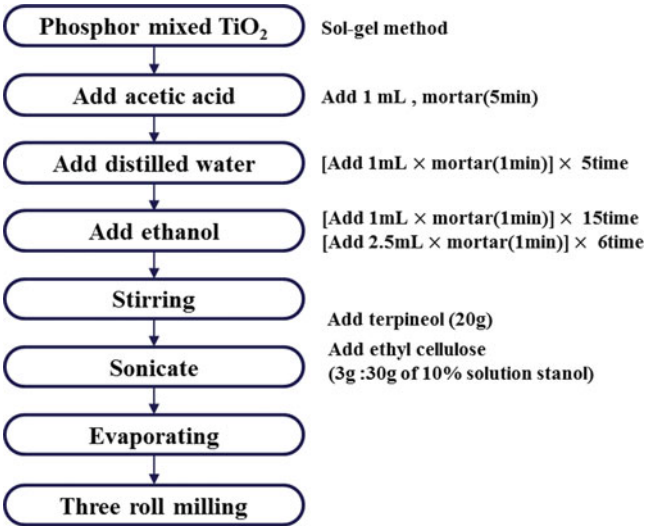

Figure 1. Flowchart for the preparation of the phosphor mixed TiO_2 paste.

conversion luminescence. Excitation and emission spectra show that the solar ultraviolet and broad region irradiation can be reabsorbed by the dye N-719 via conversion luminescence by YAG:Ce, and the solar light harvest of DSSCs may consequently be increased. Thus, the influence of phosphor additives on the conversion efficiency of DSSC was proved.

Experimental

Preparation of YAG:Ce^{3+} Powder

YAG:Ce^{3+} phosphors were prepared using the combustion reaction method [22–23]. The starting materials for the YAG:Ce^{3+} phosphors were $Y(NO_3)_3{\cdot}6H_2O$ (99.9%, Aldrich), $Al(NO_3)_3{\cdot}9H_2O$ (99.997%, Aldrich), and $Ce(NO_3)_3{\cdot}6H_2O$ (99.999%, Aldrich). Urea (NH_2CONH_2) was used as the reagent. $Y(NO_3)_3$, $Al(NO_3)_3$, and $Ce(NO_3)_3$ solutions were dissolved into deionized water. The solution was stirred on a hot plate using a magnetic bar, in air for 30 min. The resulting solution was then heated to 100°C and stirred until it became transparent. It was then heated rapidly to 300°C to initiate combustion. The color of the solution changed to bright yellow, and a few minutes later, combustion process started, resulting in a brown gas and the precursor. The precursor was dried in air, and then, sintered at 1000°C for 2 h using an alumina crucible in a furnace.

Preparation of Electrodes of DSSC

Titanium(IV) isopropoxide (TTIP, Sigma Aldrich), ethyl alcohol, nitric acid, and de-ionized (DI) water were used as the precursors. As-prepared TiO_2 particles were calcined in air at 450°C for 1 h, using a programmable furnace, to obtain the desired stoichiometry and crystallinity. The phosphor(0.5–15.00 wt.%)-mixed TiO_2 pastes were prepared using procedures as shown in Fig. 1 [24–25]). The phosphor-mixed TiO_2 paste was coated prepared by coating it on the FTO plate by employing a doctor blade technique. The phosphor-mixed TiO_2 electrode was sintered at 500°C for 15 min in air. The phosphor-mixed TiO_2 electrodes were immersed in the dye N-719 for 24 h at room temperature. For

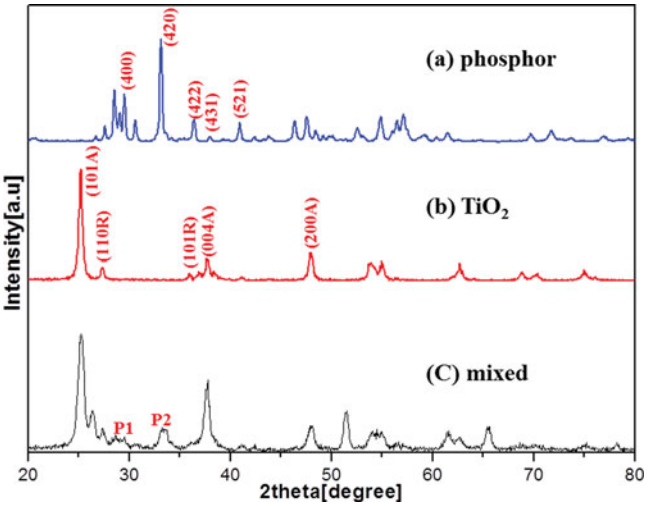

Figure 2. XRD patterns of (a) phosphor, (b) TiO_2 nanoparticle, and (c) phosphor mixed TiO_2.

comparison, a dye-sensitized TiO_2 electrode without YAG:Ce^{3+} was prepared. A counter-electrode was prepared by spin-coating H_2PtCl_6 solution onto the FTO glass and heating at 450°C for 30 min. The dye-adsorbed TiO_2 electrode and the Pt counter-electrode were assembled into a sandwich-type cell and sealed with a 60-μm-thick hot-melt sealant. An electrolyte solution was introduced through a drilled hole in the counter electrode. The hole was then sealed using a cover glass.

Measurements

The phase identification of the photoelectrode obtained was performed by X-ray diffraction (XRD) using a Rigaku D/MAX-2200 diffractometer with Cu Kα radiation. The photoluminescence (PL) spectra were recorded using a 150 W Xe lamp (spectrofluorometer, FP-6200, JASCO). The morphology of the prepared phosphor-mixed TiO_2 was investigated using field-emission scanning electron microscopy (FE-SEM, model S-4700, Hitachi). The absorption spectra of the TiO_2 electrode films were measured using a UV-vis spectrometer (UV-vis 8453, Agilent). The conversion efficiency of the fabricated DSSCs was measured using an I-V solar simulator (Solar Simulator, McScience). The active area of the resulting cell exposed to light was approximately 0.25 cm^2 (0.5 cm $\times$ 0.5 cm).

Results and Discussion

Figure 2(a) shows the XRD patterns of the YAG:Ce^{3+} phosphor. The XRD patterns show various YAG peaks and the main (420) peak. The YAG phase crystallized at a sintering temperature of 1000°C, which are in good agreement with JCPDS Card (no. 33–0040). Figure 2(b) shows the XRD pattern of the TiO_2 nanoparticles at 500°C, which indicates a mixture of the anatase and rutile phases. The XRD pattern of TiO_2 nanoparticles shows prominent (101), (004), and (200) anatase peaks, and prominent (110) and (101) rutile peaks. In the phosphor phase, the XRD patterns shown in Fig. 2(c) were observed, showing that the phosphor-mixed TiO_2 surface can efficiently crystallize the form (P1-P2).

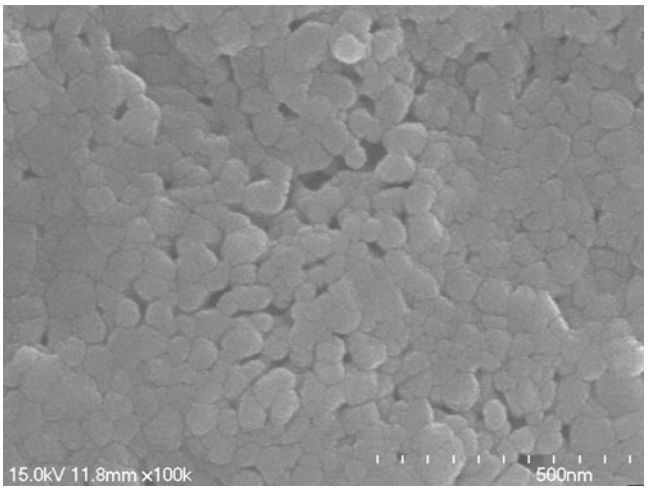

Figure 3. SEM images of the YAG:Ce^{3+} phosphor.

Figure 3 shows the SEM images of the YAG:Ce^{3+} phosphor. Uniform and spherical YAG:Ce^{3+} phosphor nanoparticles with a homogeneous structure were obtained using the combustion method at 1000°C. It can be seen that the particle size is about 50 nm. The nanometer-size crystals are suitable for inducing photoluminescence [26–27].

Figure 4 shows the excitation spectrum and emission spectra of phosphor-mixed TiO_2. It can be seen from the Fig. 4(a) that two excitation bands appear with peak wavelengths of 340 and 470 nm. There is one electron in the 4f state of Ce^{3+}, and the ground state of Ce^{3+} is split into $^2F_{7/2}$ and $^2F_{5/2}$ [28–29]. The excitation absorption band implies that solar ultraviolet irradiation can be absorbed by YAG:Ce^{3+}. Figure 4(b) shows the emission spectra of phosphor-mixed TiO_2. It can be seen that YAG:Ce^{3+} exhibits an obvious luminescence function. The emission spectrum of YAG:Ce^{3+} shows a single intense broad emission band ranging from 500 to 700 nm with a peak at 520 nm. This emission corresponds to the transition from the 5d excited state to the 4f ground state of the Ce^{3+} ion in the YAG crystal [28–29]. The luminescence at 520 nm is just within the absorption wavelength range of sensitizing dye N-719 [20–21]. Excitation and emission spectra show that the

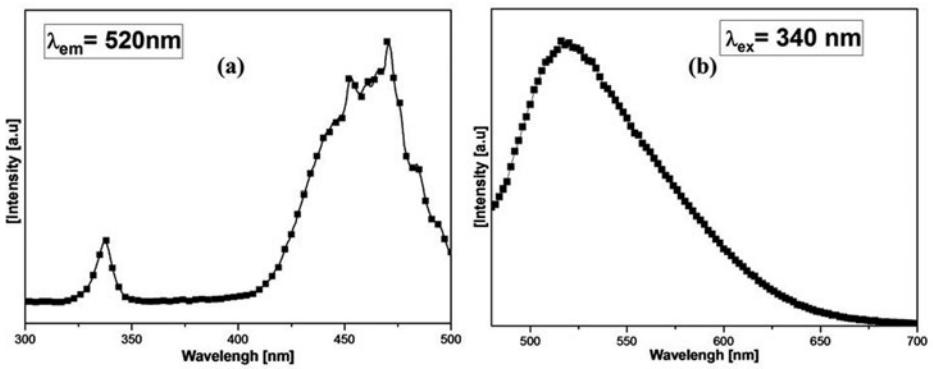

Figure 4. (a) PL excitation spectrum and (b) PL emission spectra of phosphor mixed TiO_2.

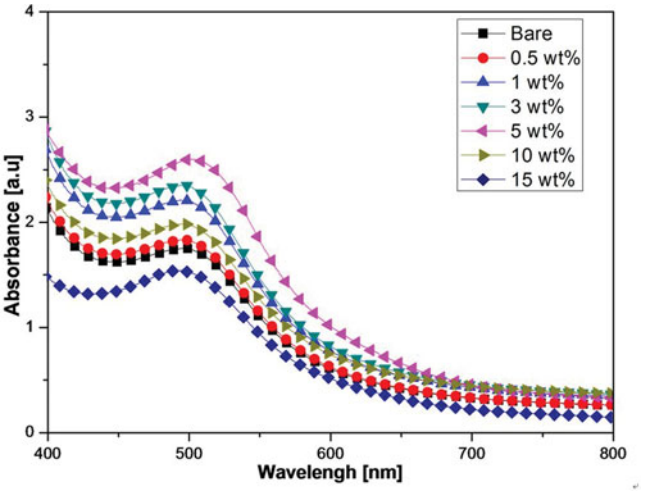

Figure 5. UV-vis absorbance of DSSCs with phosphor mixed TiO_2 for different phosphor content.

solar ultraviolet and broad region irradiation can be reabsorbed by the dye N-719 via the conversion luminescence of YAG:Ce^{3+}, and the solar light harvest of DSSC may thus be increased.

Figure 5 shows the UV-vis absorbance of the mixing phosphor ratio for the phosphor-mixed TiO_2. It can be seen in Fig. 5 that in the 400–800 nm wavelength range, the absorbance spectra for the sample with a phosphor content of 5.0 wt% was the highest. Figure 5 shows that in the range 400–800 nm, the absorbance spectra for the DSSC with phosphor-mixed TiO_2 is higher than that without phosphor-mixed TiO_2. Obviously, this is due to the conversion luminescence of phosphor and the consequent reabsorption by the dye in the DSSC.

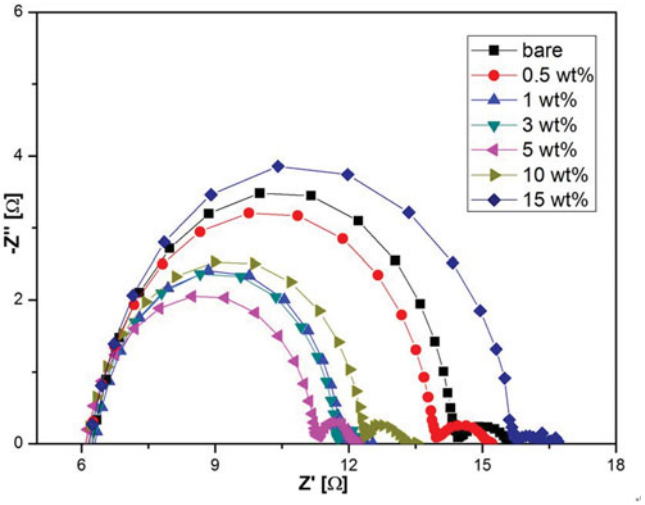

Figure 6. EIS Nyquist plots of DSSCs with phosphor mixed TiO_2 for different phosphor content.

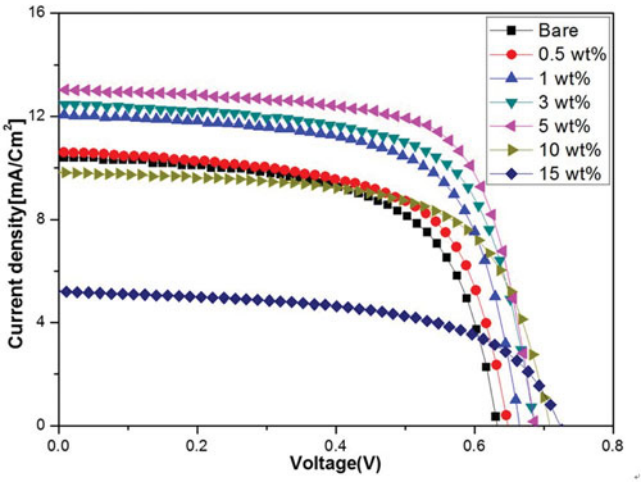

Figure 7. Photovoltaic parameters of DSSC.

Figure 6 shows electrochemical impedance spectroscopy (EIS) Nyquist plots of DSSCs with phosphor-admixed TiO_2 electrode. EIS is a useful method for the analysis of charge-transport processes and internal resistances [30]. As shown in Fig. 6, there is a decrease in the charge-transfer resistance (R_{ct}) upon increasing phosphor amount varying from 0% to 5%. This increases the number of injected electrons into the TiO_2 layer, improves the electrical conductivity, and reduces the charge recombination at the TiO_2/dye/electrolyte interface [31–32]. R_{ct} directly affects the fill factor (FF) of a DSSC. If R_{ct} decreases, FF increases and, consequently, the efficiency of the cell also increases [33].

Figure 7 shows the current–voltage photovoltaic performance curves of the DSSC with the pure TiO_2 and that with the phosphor-mixed TiO_2 under AM 1.5 illumination (100 mW/cm^2). Table 1 summarizes the efficiency, fill factor(FF), open-circuit voltage(V_{oc}), and short-circuit current (J_{sc}) for the corresponding solar cells. V_{oc} of the DSSCs depends on the energy level of the electrons in the oxide film and the redox potential of the electrolyte. If Ce^{3+} ions substitute Ti^{4+} ions at the Ti-lattice sites in TiO_2, the electronic energy level of the oxide film is elevated, which leads to an increase of V_{oc} . J_{sc} [34] increased significantly based on the effects of the mixed phosphor. As shown in Table 1, J_{sc} increases with the amount of phosphor until the phosphor content is 5.0 wt%, beyond which J_{sc} decreases. The increase in J_{sc} is mainly due to the conversion luminescence of phosphor, which facilitates

Table 1. J_{sc}, V_{oc}, FF, and efficiency

	J_{sc} (mA/cm^2)	V_{oc} (V)	FF (%)	Efficiency (η)
Bare	10.42	0.63	61.90	4.08
Wt.% 0.50	10.63	0.64	63.53	4.37
Wt.% 1.00	12.06	0.66	66.17	5.30
Wt.% 3.00	12.48	0.68	66.29	5.68
Wt.% 5.00	13.03	0.68	69.75	6.24
Wt.% 10.0	9.83	0.70	65.08	4.53
Wt.% 15.0	5.20	0.72	57.69	2.17

the harvest of more incident light [35]. The decrease in J_{sc} is due to the fact that introduction of rare-earth oxides produces defects in the oxide film, which causes the recombination of photo-induced holes and electrons [36]. Thus, we used phosphor-mixed (5.0 wt%) TiO_2 in the DSSC and realized a light-to-electric energy conversion efficiency of 6.24%, a short-circuit current density of 13.03 mA/cm^2, an open-circuit voltage of 0.68 V, and a fill factor of 69.75%. Higher efficiencies were achieved for DSSCs with phosphor-mixed TiO_2 than for the cells with pure TiO_2 nanoparticles.

Conclusions

The photovoltaic performances of DSSCs with phosphor-mixed TiO_2 (0.5–15.00 wt%) were compared. Excitation and emission spectra show that the solar ultraviolet and broad region irradiation from the sun can be reabsorbed by the dye via the conversion luminescence of YAG:Ce^{3+}, and the solar light harvest of DSSCs may thus be increased. The higher J_{sc} is related to increased harvest of incident light. Thus, conversion luminescence of phosphor improves both the light harvest and the photocurrent production. R_{ct} directly affects the FF of a DSSC. If R_{ct} decreases, FF increases and, consequently, the efficiency of the cell also increases. With 5.00 wt% of YAG:Ce^{3+}-mixed TiO_2 electrode, the light-to-electric energy conversion efficiency of the DSSC reaches 6.24% under a simulated solar light irradiation at 100 mW/cm^{-2}, which is higher by a factor of 1.52 than that of the DSSCs without YAG:Ce^{3+}-mixed TiO_2. The DSSCs based on phosphor-mixed TiO_2 show better photovoltaic performance than the cells with pure TiO_2 nanoparticles.

Funding

This work was supported by the Human Resources Development program (No. 20124030200010) of the Korea Institute of Energy Technology Evaluation and Planning (KETEP) grant funded by the Korea government Ministry of Trade, Industry and Energy and by the National Research Foundation of Korea (NRF) Grant funded by the Korean Government (MEST) (No. 2012R1A1A2044472).

References

[1] Grätzel, M. (2004). *J. Photochem. Photobiol. A*, *164*, 3.
[2] O'Regan, B., & Grätzel, M. (2004). *Nature*, *353*, 737.
[3] Chappel, S., Chen, S. G., & Zaban, A. (2002). *Langmuir*, *18*, 3336.
[4] Bedja, I., Kamat, P. V., Hua, X., Lappin, A. G., & Hotchandani, S. (1997). *Langmuir*, *13*, 2398.
[5] Keis, K., Bauer, C., Boschloo, G., Hagfeldt, A., Westermark, K., Rensmo, H., Siegbahn, H., & Photochem, J. (2002). *Photobiol. Chem.*, *148*, 57.
[6] Chappel, S., & Zaban, A. (2002). *Solar Energy Mater. Solar Cells*, *71*, 141.
[7] Guo, P., & Aegerter, M. A. (1999). *Thin Solid Films*, *351*, 290.
[8] Xia, J., Masaki, N., Jiang, K., Wada, Y., & Yanagida, S. (2006). *Chem. Lett.*, *35*, 252.
[9] Grätzel, M. (2005). *Inorg. Chem.*, *44*, 6841.
[10] Hamann, T. W., Jensen, R. A., Martinson, A. B. F., Ryswyk, H. V., & Hupp, J. T. (2008). *Energ. Environ. Sci.*, *1*, 66.
[11] Kong, F. T., Dai, S.-Y., & Wang, K. J. (2007). *Adv. Opto. Elect.*, 75384.
[12] Prakash, T. (2012). *Electronic Materials Letters, 8*, 231–243.
[13] Huh, P., & Kim, S. C. (2012). *Electronic Materials Letters*, *8*, 131–134.
[14] Hara, K., Tachibana, Y., Ohga, Y., Shinpo, A., Suga, S., Sayama, K., Sugihara, H., & Arakawa, H. (2003). *Solar Energy Materials and Solar Cells*, *77*, 89.

[15] Matsui, H., Okada, K., & Kawashima, T., *et al.* (2004). *A, Chemistry*, *164*, 129.
[16] Kim, S. S., Nah, Y. C., Noh, Y. Y., Jo, J., & Kim, D. Y. (2006). *Electrochimica Acta*, *51*, 3814.
[17] Oelhafen, P., & Schuler, A. (2005). *Solar Energy*, *79*, 110–121.
[18] Yang, Guangtao, Zhang, Jing, Wang, Peiqing, Sun, Qiang, Zheng, Jun, & Zhu, Yuejin. (2011). *Current Applied Physics*, *11*, 376–381.
[19] Wang, Yuanzhe, Chen, Enlong, Lai, Hongmei, Lu, Bin, Hu, Zhijuan, Qin, Xiaomei, Shi, Wangzhou, & Guoping, Du. (2013). *Ceramics International*, *39*, 5407–5413.
[20] Gratzel, M. (2001). *Nature*, *414*, 338.
[21] Shen, Heping, Li, Xin, Li, Jianbao, Wang, Wenli, & Lin, Hong. (2013). *Electrochimica Acta*, *97*, 160–166.
[22] Lee, S. K., Yoon, H. H., Park, S. J., Kim, K. H., & Choi, H. W. (2007). *Japanese Journal of Applied Physics*, *46*, 7983–7986.
[23] Kwak, H. H., Kim, S. J., Yoon, H. H., Park, S. J., & Choi, H. W. (2009). *Journal of Electroceramics*, *23*, 397–401.
[24] Jin, Y. S., Kim, K. H., Park, S. J., Yoon, H. H., & Choi, H. W. (2011). *J. Nanosci. Nanotechnology, 11*, 10971–10975.
[25] Jhon, D., Nico, A., & Sommerdijk, J. M. (2001). *Gordon and Breach Science Publishers*.
[26] Fadlalla, H. M. H., Tang, C. C., Elssfah, E. M., & Shi, F. (2008). *Materials Chemistry and Physics 109*, 436–439.
[27] Li, Xia, Liu, Hong, Wang, Jiyang, Cui, Hongmei, & Han, Feng. (2004). *Materials Research Bulletin 39*, 1923–1930.
[28] Rodríguez-Rojas, R. A., De la Rosa-Cruz, E., Díaz-Torres, L. A., Salas, P., Meléndrez, R., Barboza-Flores, M., Meneses-Nava, M. A., & Barbosa-García, O. (2004). *Opt. Mater.*, *25*, 285.
[29] Yang, Zhiping, Li, Xu, Yang, Yong, & Li, Xingmin. (2007). *Journal of Luminescence, 122–123*, 707–709.
[30] Yang, C. C., Zhang, H. Q., & Zheng, Y. R. (2011). *Current Applied Physics Supplement*, *11*, S147–S153.
[31] Fabregat-Santiago, F., Bisquert, J., Palomares, E., Otero, L., Kuang, D., Zakeeruddin, S. M., & Grätzel, M. (2007). *J. Phys. Chem. C*, *111*, 6550–6560.
[32] Kern, R., Sastrawan, R., Ferber, J., Stangl, R., & Luther, J. (2002). *Electrochim. Acta*, *47*, 4213–4225.
[33] Gagliardi, S., Giorgi, L., Giorgi, R., Lisi, N., Dikonimos Makris, Th., Salernitano, E., & Rufoloni, A. (2009). *Superlattices and Microstructures 46*, 205–208.
[34] Ko, K., Lee, Y., & Jung, Y. (2005). *J. Colloid Interface Sci.*, *283*, 482.
[35] Chou, C. S., Guo, M. G., Liu, K. H., & Chen, Y. S. (2012). *Applied Energy*, *92*, 224–233.
[36] Murakoshi, K., Kano, G., Wada, Y., Yanagida, S., Miyazaki, H., Matsumoto, M., & Murasawa, S. (1995). *J. Electroanal. Chem.*, *396*, 27.